International Journal of Nanomedicine

Dovepress

open access to scientific and medical research

Open Access Full Text Article

ORIGINAL RESEARCH

Lactosylated IR820/DOX Co-Assembled Nanodrug for Synergetic Antitumour Therapy

This article was published in the following Dove Press journal:
International Journal of Nanomedicine

Yue Jiang[1]
Chunzhi Huang[1,2]
Yuxia Luan[1]

[1]Department of Pharmaceutics, Key Laboratory of Chemical Biology (Ministry of Education), School of Pharmaceutical Sciences, Shandong University, Jinan, Shandong Province, People's Republic of China; [2]Department of Pharmacy, Third Affiliated Hospital of Zhengzhou University, Zhengzhou, People's Republic of China

Introduction: Synergistic treatment integrating photothermal therapy (PTT) and chemotherapy is a promising strategy for hepatocellular carcinoma (HCC). However, the most commonly used photothermal agent, IR820, and chemotherapeutic drug, doxorubicin hydrochloride (DOX), are both hydrophilic molecules that suffer from the drawbacks of a short circulation time, rapid elimination and off-target effects.

Methods and Results: Herein, a novel nanodrug that combined HCC-targeted IR820 and DOX was developed based on excipient-free co-assembly. First, lactosylated IR820 (LA-IR820) was designed to target HCC. Then, the LA-IR820/DOX nanodrug (LA-IR820/DOX ND) was purely self-assembled without excipient assistance. The physicochemical properties and the chemo-photothermal antitumour activity of the excipient-free LA-IR820/DOX ND were evaluated. More importantly, the obtained LA-IR820/DOX ND exhibited 100% drug loading, remarkable HCC targeting and excellent antitumour efficacy.

Conclusion: This excipient-free LA-IR820/DOX ND may be a promising candidate for the synchronous delivery and synergistic targeting of IR820 and DOX as a combined chemo-photothermal therapy.

Keywords: excipient-free, hepatoma cell targeting, self-assembly nanodrug, photothermal therapy, chemotherapy

Introduction

Hepatocellular carcinoma (HCC) is one of the leading causes of cancer-related death throughout the world.[1,2] Its insidious onset, rapid progress and severe liver dysfunction lead to high mortality.[3] To date, commonly used anthracyclines have been unsatisfactory in the treatment of advanced HCC patients, whose survival time is only three to four months in most Asian countries.[4,5] Therefore, there is an urgent need to explore more efficient and safer treatments for HCC. Photothermal therapy (PTT) employs optical absorbing agents to induce local hyperthermia to ablate tumours by near-infrared (NIR) light irradiation.[6] It has attracted significant attention due to its non-invasiveness, high spatiotemporal selectivity and limited therapeutic resistance.[7] Remarkably, in addition to causing direct tumour cell death, PTT can also decrease interstitial fluid pressure and increase blood perfusion.[8,9] Moreover, the destruction of cancer cells by hyperthermia causes immunogenic cell death (ICD), which can release tumour-specific antigens to initiate the antitumour immune response.[10,11] However, PTT alone is insufficient to eradicate tumours due to the limited penetration depth of NIR light. The surviving tumour cells from PTT will continue to proliferate, leading to cancer recurrence and metastasis.[12,13]

Correspondence: Yuxia Luan
Department of Pharmaceutics, Key Laboratory of Chemical Biology (Ministry of Education), School of Pharmaceutical Sciences, Shandong University, 44 Wenhuaxi Road, Jinan, Shandong Province 250012, People's Republic of China
Tel +86 531-88382007
Fax +86 531-88382548
Email yuxialuan@sdu.edu.cn

submit your manuscript | www.dovepress.com
DovePress
http://doi.org/10.2147/IJN.S247617

From this viewpoint, it is essential to combine other therapeutic strategies with PTT in a coordinated way. The combination of PTT and chemotherapy has been shown to be an encouraging approach resulting in superior synergistic effects and lower side effects.[14–17] The introduction of chemotherapy provides an opportunity to kill deep tumour cells, and some chemotherapeutic agents, such as DOX, can also induce ICD, consolidating the antitumour immunity invoked by PTT. Some challenges, however, still need to be overcome to achieve the optimal therapeutic effect. In many reported systems, IR820 and DOX are commonly used small hydrophilic molecules.[18,19] However, their theranostic effect is limited due to shortcomings such as instability, short lifetime, rapid elimination and non-specific tumour-homing ability.[20–22] It is therefore, highly desirable to exploit an IR820 and DOX co-assembled nanosystem that provides increased stability, tumour targeting and prolonged circulation time.

In recent years, tremendous efforts have been made to develop nanodrug delivery systems, which are anticipated to optimize cancer therapy.[23–25] Among them, self-assembly has attracted considerable interest due to its facile fabrication and flexibility in the organization of ordered nanostructures. Nevertheless, excipient-assistant nanodrugs suffer from low drug-loading capacity (< 20%), native toxicity of excipients and difficulty in scaling up production, all of which hinder their commercialization.[26] To address these concerns, the innovative drug delivery system of excipient-free nanodrugs self-assembled by active small molecules without inert excipients have been developed and attracted extensive attention.[27–29] Excipient-free nanodrugs can simultaneously achieve high drug-loading efficiency, display good pharmacokinetics and avert the safety problems caused by excipients.[30,31] Shim et al developed a excipient-free DOX prodrug, in which the cathepsin B-cleavable peptide was conjugated to DOX for tumour targeting, tumour-specific DOX release and reduction of systemic toxicity.[26] However, the types of tumour-responsive linkers are limited and the conjugation often needs tedious synthesis. Fan et al reported a excipient-free nanodrug formed by pure ursolic acid to treat the nonsmall cell lung cancer.[32] Feng et al reported an indocyanine green (ICG)-templated self-assembly of paclitaxel (PTX), achieving 90.7% PTX and 9.2% ICG loading.[28] This co-assembly nanosystems may offer new inspiration for synergistic therapy. However, the pure and co-assembly nanodrug both suffer from certain systemic toxicity due to the lack of active targeting. Therefore, it is essential to develop an active targeting excipient-free self-assembly for synergistic therapy. Because the asialoglycoprotein receptor (ASGPR) is exclusively expressed in hepatoma cells and can recognize and internalize glycoproteins bearing terminal lactose moieties, we previously developed a lactosylated IR820 (LA-IR820) that enabled HCC targeting.[33] Here, we developed an excipient-free nanodrug composed of only the HCC-targeted IR820 and chemotherapeutic DOX via pure self-assembly. The physicochemical properties and the chemo-photothermal antitumour activity of the excipient-free LA-IR820/DOX nanodrug (LA-IR820/DOX ND) were evaluated. The results revealed that LA-IR820/DOX ND displayed 100% drug loading, remarkable HCC targeting and excellent antitumour efficacy. Thus, this excipient-free LA-IR820/DOX ND may be a promising candidate for targeted chemo-photothermal therapy against hepatocellular carcinoma.

Experimental Section

Materials

IR820 was purchased from Beijing J & K Technology Co., Ltd. (China). Lactobionic acid was supplied by Sigma-Aldrich (USA). Doxorubicin hydrochloride (DOX) was obtained from Dalian Meilun Biological Technology Co., Ltd. (China). Trypan blue was received from Beijing Solarbio Technology Co., Ltd. (China). Methylene dichloride (>99.5, CH_2Cl_2) and triethylamine (Et_3N, >99.0%, $(C_2H_5)_3N$) were provided by Tianjin Fuyu Fine Chemical Co., Ltd. (China).

Preparation of LA-IR820/DOX ND

LA-IR820 was synthesized as previously described.[33] The self-assembly process of LA-IR820 and DOX is illustrated in Figure 1A. Briefly, LA-IR820 (1 mM, 1.0 mL) and DOX (2 mM, 1.0 mL) were individually dissolved in distilled water, and the DOX solution was added dropwise to LA-IR820 solution with 200 rpm stirring, and yielding spherical LA-IR820/DOX ND.

Morphology of LA-IR820/DOX ND

Transmission electron microscopy (TEM, JEM-200CX II, Electronics Corporation, Japan) and dynamic light scattering (DLS, Zetasizer Nano ZS, Malvern Panalytical, England) were used to characterize the morphology and particle size of LA-IR820/DOX ND. The UV-visible absorption spectra of IR820 and LA-IR820 were recorded

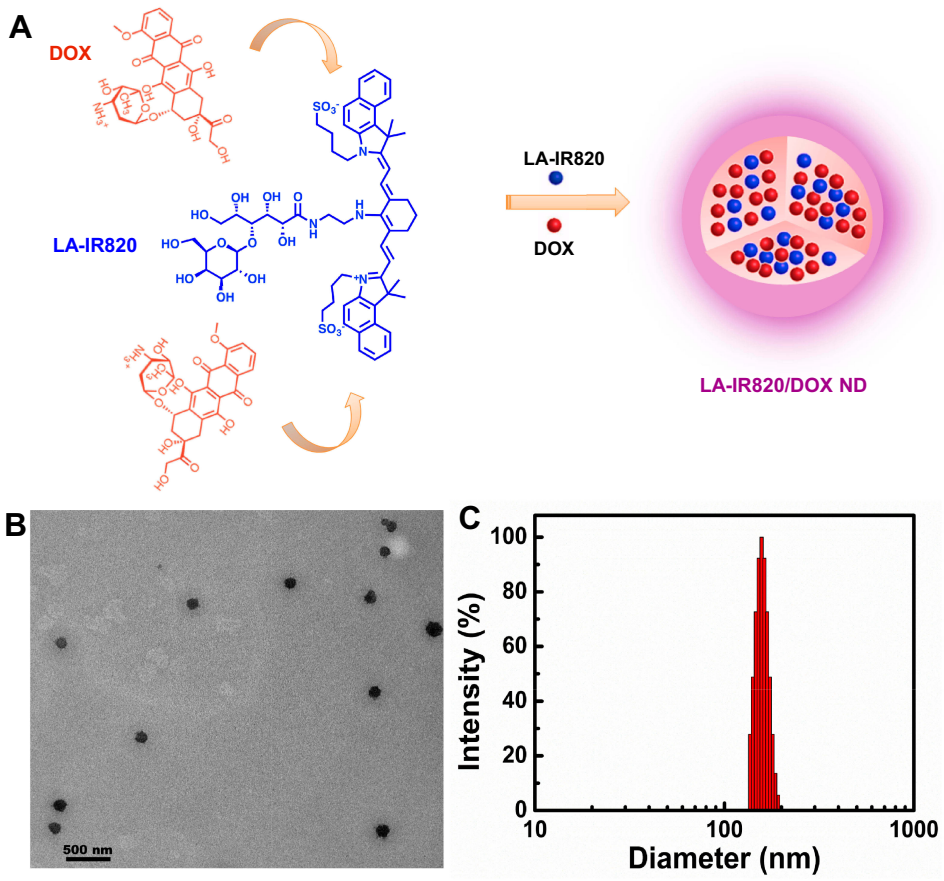

Figure 1 (**A**) Schematic representation of the self-assembly process of LA-IR820/DOX ND with the molar ratio of 1:2 (LA-IR820:DOX); (**B**) TEM image of LA-IR820/DOX ND, and the scale bar is 500 nm; (**C**) size distribution of LA-IR820/DOX ND.

by UV-visible spectrophotometer (TU-1810, General Analysis Instrument Co., Ltd., China). All samples were tested at room temperature.

In vitro Drug Release Studies

The DOX release from LA-IR820/DOX ND was studied using the dialysis method. One millilitre of LA-IR820/DOX ND (c = 150 μg/mL) was put into the dialysis bag (MWCO ~ 3500 Da) and incubated at 37.0 ± 0.5 °C in 20 mL PBS (pH 7.4) with 100 rpm stirring. At specific time points, 1.0 mL of the release medium was taken out and replaced with the same volume of fresh medium. The content of DOX was analysed using a fluorescence spectrophotometer at an excitation wavelength of 496 nm and an emission wavelength of 558 nm. The accumulated DOX release was calculated by the following equation:

$$\text{Cumulative release amount}(\%) = M_t/M_{\text{total}} \times 100\%$$

where M_t is the amount of DOX released into the medium at time point t, and M_{total} is the total amount of DOX in the dialysis bag.

In vitro Photothermal Performance

The photothermal effect of IR820 and LA-IR820/DOX ND was conducted using distilled water as a control, and the concentrations of the photothermal agents ranged from 10 μM to 100 μM. One millilitre of IR820 and LA-IR820/DOX ND were added to a 12-well plate and irradiated at 808 nm (1.0 W·cm^{-2}) and 660 nm (1.0 W·cm^{-2}), respectively, for 5 min. During laser irradiation, the temperature was monitored every 30 seconds.

Cell Culture

Human HepG2 hepatoma cells and murine Hepa1-6 hepatoma cells were purchased from American Type Culture Collection (ATCC). HepG2 cells were cultured in RPMI-1640 medium (Gibco, Thermo Scientific, USA) and Hepa1-6 cells were cultured in high glucose DMEM (Gibco, Thermo Scientific, USA) at 37 °C with 5% CO_2. Both mediums contained 10% foetal bovine serum (Qingdao Haosail Technology Co., Ltd, China) and 1% penicillin-streptomycin antibiotic mixture (Beijing solarbio science and technology co., Ltd, China).

Intracellular Uptake of LA-IR820/DOX ND

HepG2 cells (2×10^5 cells/well) were incubated in a 6-well plate for 24 h. Then, the medium was removed and replaced with the medium containing free DOX, IR820 and DOX co-assembly nanodrug (IR820/DOX ND) and LA-IR820/DOX ND, respectively (DOX: 10 μg/mL). After 4 h incubation, the medium was discarded, and the cells were rinsed three times with pH 7.4 PBS. Then, the cells were analysed by fluorescence inverted microscopy (ECLIPSE-Ti, Nikon, Japan) and flow cytometry (BD FACSAria III, USA).

Cytotoxicity Assay

Hepa1-6 and HepG2 cells were chosen to estimate the dark cytotoxicity of IR820 and LA-IR820 by the methyl tetrazolium (MTT) method. Hepa1-6 and HepG2 cells were seeded in 96-well plates at a density of 5×10^3 cells for overnight incubation. Afterwards, the medium was replaced with fresh medium containing IR820 and LA-IR820 at concentrations ranging from 0.076 μM to 38 μM. After 24 h, 20 μL MTT (5%) was added into each well for another 4 h incubation. The supernatants were then discarded and 150 μL DMSO was added to each well to dissolve formazan crystals. The absorbance was measured by PerkinElmer ELISA at a test wavelength of 570 nm.

To evaluate the chemo-photothermal antitumour efficacy, cells were incubated with different concentrations of DOX, IR820, LA-IR820 and LA-IR820/DOX ND with equivalent DOX (c = 0.1, 1, 10, 20, and 50 $\mu g \cdot mL^{-1}$) for 4 h. Subsequently, the drug-containing medium was substituted by the fresh drug-free medium. The cells treated with IR820 were irradiated by an 808 nm laser while the LA-IR820 and LA-IR820/DOX ND-treated cells were irradiated by a 660 nm laser at a power of 1.0 $W \cdot cm^{-2}$ for 2 min. After 24 h, the cytotoxicity was tested by MTT. The cell inhibition ratio was calculated by the following formula:

$$\text{Cell inhibition ratio}(\%) = \left(1 - \frac{A_{\text{sample}}}{A_{\text{negative}}}\right) \times 100\%$$

where A_{sample} and $A_{negative}$ are the absorbance values from each sample and negative control, respectively.

Trypan Blue Staining

Trypan blue staining can directly determine whether cells are alive. HepG2 cells (5×10^4 cells) were seeded in 24-well plates and incubated overnight. Then, the medium was substituted for fresh medium with free DOX, IR820 and LA-IR820/DOX ND with the same DOX concentration (50 $\mu g \cdot mL^{-1}$). After incubation for 4 h, the medium was replaced with drug-free medium and the photothermal agent-treated cells received irradiation at 808 nm or 660 nm at a power of 1.0 $W \cdot cm^{-2}$ for 2 min. After another 24 h, the cells were rinsed with fresh PBS, digested and suspended. Then, the cells were observed under a microscope (NIKON Ti-U, Japan) after trypan blue staining.

Haemolysis Test

The biocompatibility of LA-IR820/DOX ND was evaluated by determining the haemolysis ratio (HR). Firstly, 2% (v/v) red cell suspension was prepared. Normal saline (1.1 mL) and 1.25 mL red cell suspension were mixed and then 0.15 mL LA-IR820/DOX ND was added with DOX concentrations ranging from 1 $\mu g \cdot mL^{-1}$ to 100 $\mu g \cdot mL^{-1}$. Each sample was bathed at 37 °C for 3 h and then centrifuged at 1500 rpm for 15 min. The supernatant was collected and absorbance was measured at 576 nm with a UV-visible spectrophotometer. Red cell suspension (1.25 mL) mixed with 1.25 mL distilled water was used as the positive control, and 1.25 mL red cell suspension mixed with 1.25 mL normal saline was the negative control. Counteracting the interference absorption of LA-IR820 at 576 nm, equivalent LA-IR820 samples with different concentrations were prepared. The 2% red cell suspension was replaced by an equal volume of normal saline, and the other steps were conducted under the same conditions. The absorbance difference between LA-IR820/DOX ND and LA-IR820 was considered the true absorbance of each sample. HR was counted as follows:

$$\text{HR}(\%) = \frac{A_{\text{sample}} - A_{\text{negative}}}{A_{\text{positive}} - A_{\text{negative}}} \times 100\%$$

where A_{sample} $A_{negative}$ and $A_{positive}$ are the absorbances from each sample, negative control and positive control, respectively.

Statistical Analysis

Data were expressed as the mean ± SD and analysed by nonlinear regression using GraphPad Prism 7.0 software.

Results and Discussion

The HCC-targeted LA-IR820 was synthesized according to our previous report.[32] The assembly process of LA-IR820/DOX ND is presented in Figure 1A. We obtained LA-IR820/DOX ND through a simple procedure that only required

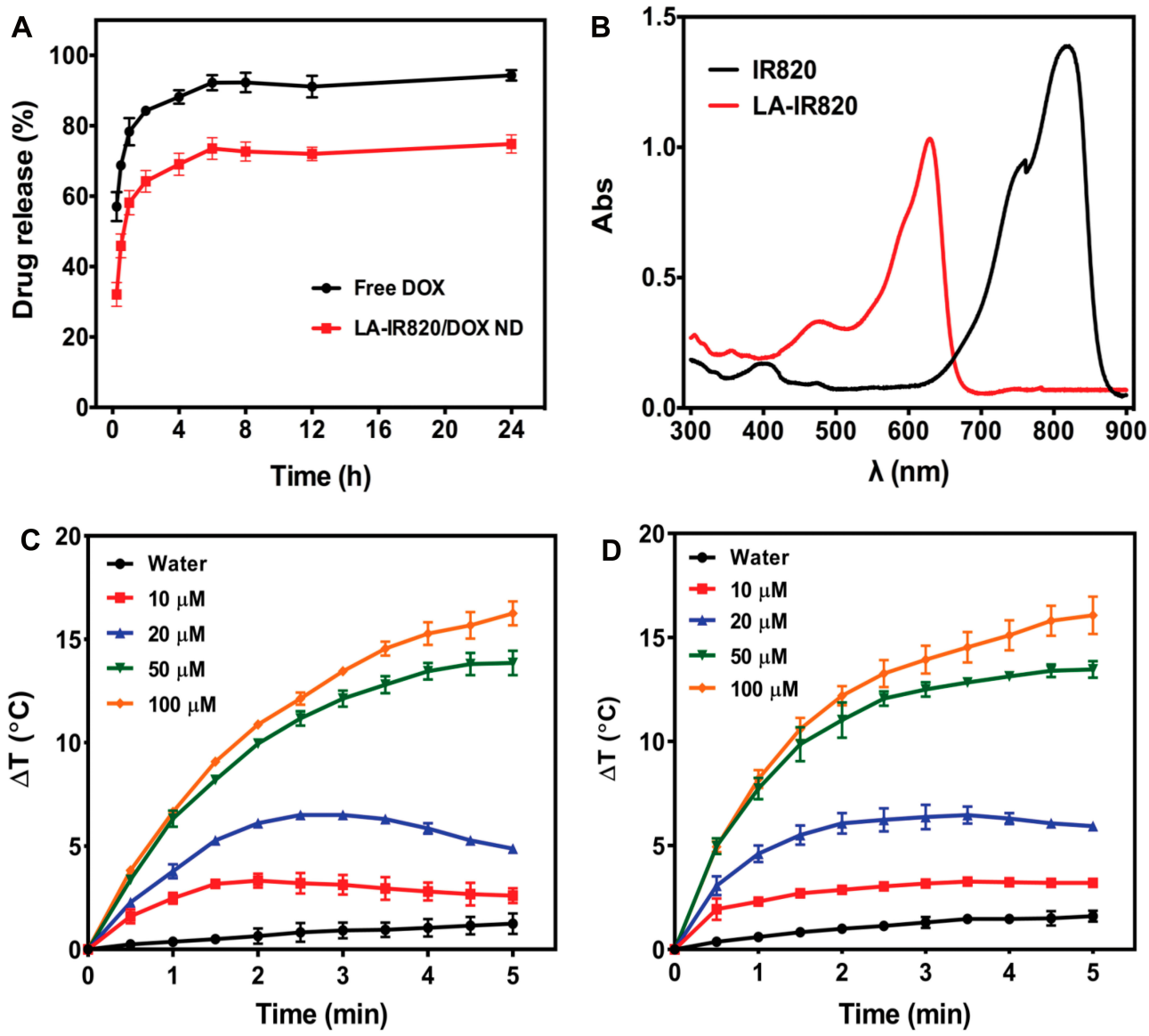

Figure 2 (**A**) The release curves of free DOX and LA-IR820/DOX ND in pH 7.4 PBS; (**B**) the UV-visible spectra of IR820 and LA-IR820; temperature increase profiles of different concentrations of (**C**) IR820 and (**D**) LA-IR820/DOX ND after irradiation with a laser wavelength of 808 nm and 660 nm, respectively (P = 1.0 W·cm^{-2}, n = 3).

mixing the two components in an aqueous solution. To determine the morphology of aggregates, TEM was used. The appearance of spherical nanoparticles in the TEM image proved the successful self-assembly of LA-IR820/DOX ND without any excipients (Figure 1B). The organization of the ordered nanostructures was most likely driven by π-π stacking interactions, hydrogen bonds, electrostatic interactions, and hydrophobic interactions. The hydrophobic aromatic ring structures of LA-IR820 and DOX can induce the formation of hydrophobic cores through hydrophobic interactions and π-π stacking interactions. At the same time, the hydrophilic fragment sticks out of the core to further stabilize the formed nanostructure. This 100% drug-loaded system contained 48.9 wt % LA-IR820 and 51.1 wt % DOX, which are much higher values than those of excipient-assisted nanosystems. DLS was further used to survey the size and size distribution. As shown in Figure 1C, the hydrodynamic diameter of LA-IR820/DOX ND was 174.0 ± 10.2 nm with quite a narrow PDI of 0.169. Zeta potential of LA-IR820/DOX ND was −15.33 mV. Previous studies have shown that 10–200 nm nanoparticles can passively target tumour sites through the enhanced permeability and retention (EPR) effect.[34] Therefore, our LA-IR820/DOX ND is appropriate for both passive and active tumour targeting.

The release behaviour of DOX from LA-IR820/DOX ND was investigated in PBS, pH 7.4. Release profiles are

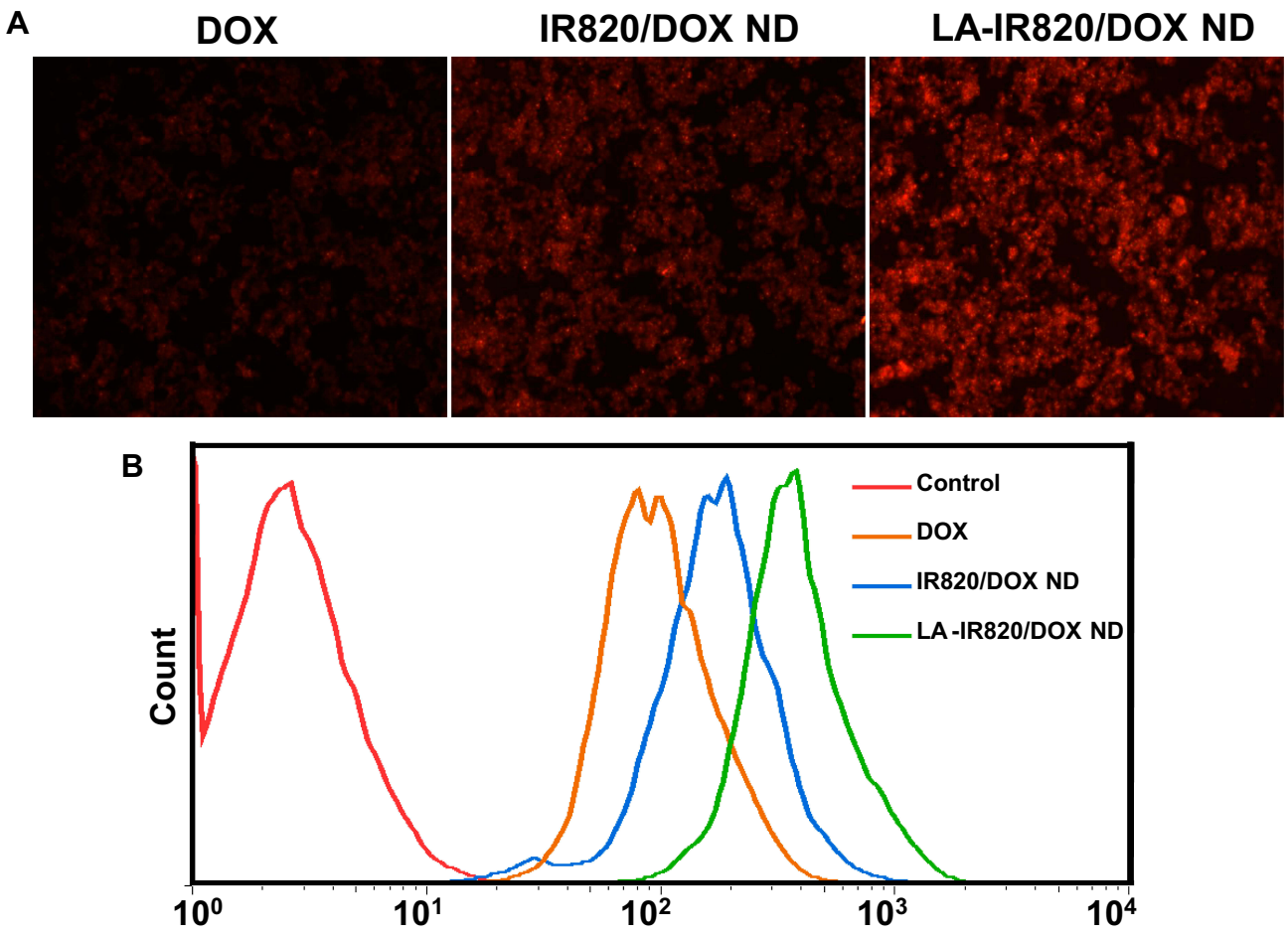

Figure 3 Intracellular uptake of DOX, IR820/DOX ND and LA-IR820/DOX ND in HepG2 hepatoma cells: (**A**) fluorescence microscopy images, (**B**) flow cytometry results.

shown in Figure 2A. The release rate of DOX from the LA-IR820/DOX ND was slower than that of free DOX. Compared to the 78.3% cumulative release of free DOX in 1 h, the LA-IR820/DOX ND did not reach achieve the same amount of DOX release in 24 h. Therefore, sustained LA-IR820/DOX ND exhibited its potential in prolonging circulation time and reducing clearance rate to a certain extent.[35–37] The UV-vis spectra (Figure 2B) show that the maximum absorption peak of IR820 was at 821 nm while the peak absorption of the HCC-targeted LA-IR820 had a blueshift to 630 nm. Therefore, using a 660 nm laser is much more reasonable for LA-IR820/DOX ND irradiation, and an 808 nm laser is suitable for IR820 irradiation. To evaluate the photothermal efficacy of LA-IR820/DOX ND in PTT, the temperature increase after laser irradiation was tested in vitro. For comparison, different concentrations of free IR820 were investigated as the control group. IR820 and LA-IR820/DOX ND were irradiated for 5 min at 808 nm and 660 nm, respectively. As illustrated in Figure 2C and D, it was obvious that the temperature-increasing capability correlated with concentration, indicating their concentration-dependent photothermal effect during the tested time interval. Notably, IR820 and the LA-IR820/DOX ND had similar photothermal efficacy under laser irradiation, which demonstrated that the lactobionic acid modification had negligible effects on the photothermal properties of IR820.

Effective intracellular uptake is a precondition for satisfactory chemotherapeutic effect of DOX. Therefore, the intracellular internalization of LA-IR820/DOX ND was investigated qualitatively and quantitatively in HepG2 hepatoma cells. In the fluorescence microscope experiment, the fluorescence of DOX was used to indicate the intracellular uptake. To verify the targeting effect of the LA-modified nanodrug, the IR820

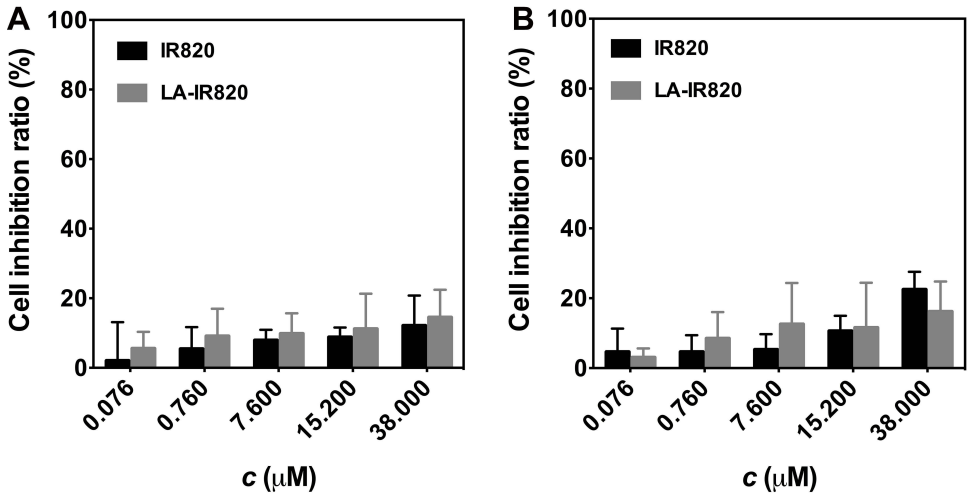

Figure 4 Dark toxicity of IR820 and LA-IR820 at various concentrations to (**A**) Hepa1-6 cells and (**B**) HepG2 cells.

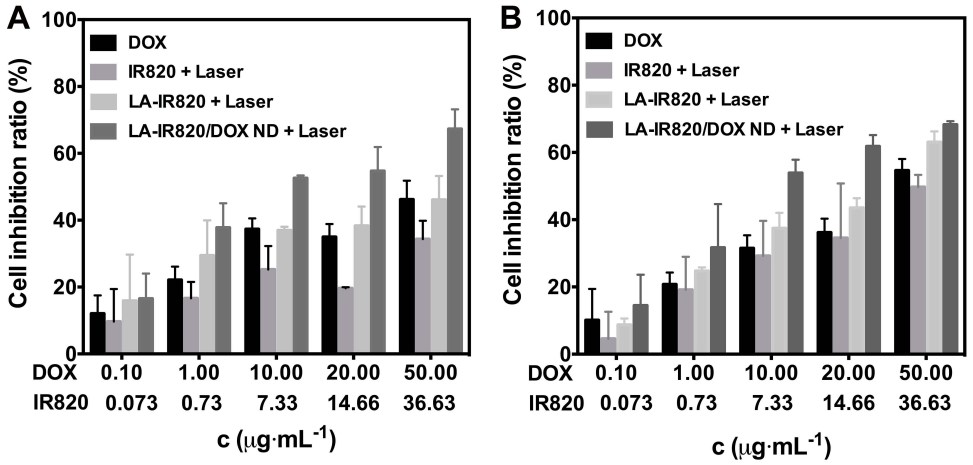

Figure 5 Cell inhibition ratio of DOX, IR820 + laser (808 nm, 1.0 W·cm^{-2}, 2 min), LA-IR820 + laser (660 nm, 1.0 W·cm^{-2}, 2 min) and LA-IR820/DOX ND + laser (660 nm, 1.0 W·cm^{-2}, 2 min) at various concentrations incubated with (**A**) Hepa1-6 cells and (**B**) HepG2 cells.

and DOX co-assembly nanodrug (IR820/DOX ND) was prepared as an untargeted control. As shown in Figure 3A, the LA-IR820/DOX ND group exhibited much stronger fluorescence intensity than not only the free DOX group but also the IR820/DOX ND group. The increased IR820/DOX ND uptake in HepG2 cells was mainly because IR820/DOX ND entered cells through endocytosis instead of passive diffusion as free DOX. More importantly, the significantly improved LA-IR820/DOX ND internalization could be attributed to the LA ligand on the surface of this nanodrug, which can bind to the overexpressed ASGP receptor on the surface of hepatoma cancer cells. Quantitative analysis by flow cytometry (Figure 3B) agreed with the qualitative analysis. Consequently, these results obviously suggested that LA-IR820/DOX ND is competent to act as both the cargo and carrier, actively targeting drug delivery into hepatic carcinoma cells and guaranteeing the efficacy of chemotherapy and PTT.

To evaluate the safety of LA-IR820, murine Hepa1-6 cells and human HepG2 cells were selected for the cytotoxicity assay. The cytotoxicity of IR820 and LA-IR820 at different concentrations was assessed in the absence of laser irradiation, and the LA-IR820 showed rather low cytotoxicity on both cell lines within the studied concentration range (Figure 4). LA-IR820 displayed a small increase in toxicity compared with IR820, which was most likely caused by improved intracellular uptake through receptor-mediated endocytosis and could also be due to the HCC-targeting property of LA. LA-IR820 would reduce the damage to

Table 1 IC_{50}[a] Values of DOX, IR820 + Laser, LA-IR820 + Laser and LA-IR820/DOX ND + Laser Against Hepa1-6 and HepG2 Cells

Cell Line	Groups	IC_{50} (μM)
Hepa1-6	DOX	175.8
	IR820 + Laser	588.5
	LA-IR820 + Laser	82.43
	LA-IR820/DOX ND + Laser	6.349
HepG2	DOX	93.19
	IR820 + Laser	59.21
	LA-IR820 + Laser	20.81
	LA-IR820/DOX ND + Laser	5.884

Note: [a]The half-maximal inhibitory concentrations.

normal cells, which suggests that LA-IR820 could be a high-safety therapeutic agent for biomedical applications. To further assess the safety of the LA-IR820/DOX ND, a haemolysis test was performed. As shown in Figure S1, the haemolysis ratios of the LA-IR820/DOX ND were all less than 5% at different concentrations, indicating its good biocompatibility and safety.

The antitumour activity of DOX, IR820 with laser, LA-IR820 with laser, and LA-IR820/DOX ND with laser was investigated. As shown in Figure 5, the antitumour ability of each group was in a dose-dependent manner. Notably, different concentrations of LA-IR820/DOX ND in the presence of laser exhibited the highest inhibition ratios of both cells among all groups. This result can be explained by the fact that the LA-IR820/DOX ND are efficiently internalized by hepatoma cells through ASGP receptor-mediated endocytosis due to the specific binding ability originating from the LA moiety. After endocytosis, DOX was released intracellularly, achieving its therapeutic effect. To quantitatively analyse the cytotoxicity, the half-maximal inhibitory concentrations (IC_{50} values) were calculated. As shown in Table 1, the IC_{50} value of IR820 was approximately 7.1 times and 2.8 times higher than that of LA-IR820 for the two cell lines under the same laser irradiation, which proved the excellent tumour targeting ability endowed by the LA motif. Specifically, the IC_{50} value of LA-IR820/DOX ND in the presence of the laser was 6.349 μM and 5.884 μM, which confirmed that LA-IR820/DOX ND could produce a marked antitumour effect under laser irradiation. The cytotoxicity of LA-IR820/DOX ND in the presence of laser was also verified by trypan blue staining (Figure S2). The results were consistent with those of the MTT assay. The maximum quantity of stained cells was observed in the LA-IR820/DOX ND with laser treatment. Therefore, synergistic antitumour activity was successfully achieved by the combination of tumour-targeted photothermal therapy and chemotherapy.

Conclusion

In summary, we developed an excipient-free nanodrug composed only of HCC-targeted IR820 and chemotherapeutic DOX via pure self-assembly. In the present study, LA-IR820 and DOX co-assembled into well-defined nanospheres with optimal size and distribution, ensuring passive tumour-targeting ability. The 100% drug loading (48.9 wt % LA-IR820 and 51.1 wt % DOX) resolved the extremely low drug loading and excipient-induced toxicity problems of excipient-assistant systems. Specifically, LA-IR820 endowed the LA-IR820/DOX ND with active targeting capability. The sustained LA-IR820/DOX ND release made it potential to prolong circulation time and reduce clearance rate of the hydrophilic IR820 and DOX. The assembled LA-IR820/DOX ND exhibited remarkably enhanced accumulation in hepatoma cells, providing an opportunity to overcome the undesirable side effects. This excipient-free synergistic nanodrug demonstrated higher antitumour activity than individual treatment with the same dose. Thus, this excipient-free LA-IR820/DOX ND may be a promising candidate for synchronous drug delivery and synergistic chemo-photothermal therapy targeting hepatoma cells.

Acknowledgments

This work was supported by the National Natural Science Foundation of China (NSFC, No. 21872083, No. 81903558), the China Postdoctoral Science Foundation (2018M642675), Shandong Provincial Natural Science Foundation (ZR2018PH043), the Fundamental Research Funds of Shandong University (2017HW0019) and the Shandong Provincial Major Science & Technology Innovation Project (2018CXGC1411).

Disclosure

The authors report no conflicts of interest in this work.

References

1. Bray F, Ferlay J, Soerjomataram I, Siegel RL, Torre LA, Jemal A. Global cancer statistics 2018: GLOBOCAN estimates of incidence and mortality worldwide for 36 cancers in 185 countries. *CA Cancer J Clin*. 2018;68:394–424. doi:10.3322/caac.21492
2. Jemal A, Bray F, Center MM, Ferlay J, Ward E, Forman D. Global cancer statistics. *CA Cancer J Clin*. 2011;61:69–90. doi:10.3322/caac.20107

3. Sainz BS, Heeschen C. Standing out from the crowd: cancer stem cells in hepatocellular carcinoma. *Cancer Cell*. 2013;23:431–433. doi:10.1016/j.ccr.2013.03.023
4. Zhang Z, Lai ECH, Zhang C, et al. The strategies for treating primary hepatocellular carcinoma with portal vein tumor thrombus. *Int J Surg*. 2015;20:8–16. doi:10.1016/j.ijsu.2015.05.009
5. Abreu RM, Ferreira CS, Nasser PD, Kikuchi LOO, Carrilho FJ, Ono SK. Hepatocellular carcinoma: the final moments of life. *J Cancer Ther*. 2013;4:377–383. doi:10.4236/jct.2013.42A045
6. Jung HS, Verwilst P, Sharma A, Shin J, Sessler JL, Kim JS. Organic molecule-based photothermal agents: an expanding photothermal therapy universe. *Chem Soc Rev*. 2018;47:2280–2297. doi:10.1039/c7cs00522a
7. Hu J, Cheng Y, Zhang X. Recent advances in nanomaterials for enhanced photothermal therapy of tumors. *Nanoscale*. 2018;10:22657–22672. doi:10.1039/c8nr07627h
8. Wang X, Li H, Liu X, et al. Enhanced photothermal therapy of biomimetic polypyrrole nanoparticles through improving blood flow perfusion. *Biomaterials*. 2017;143:130–141. doi:10.1016/j.biomaterials.2017.08.004
9. He G, Chen S, Xu Y, et al. Charge reversal induced colloidal hydrogel acts as a multi-stimuli responsive drug delivery platform for synergistic cancer therapy. *Mater Horiz*. 2019;6:711–716. doi:10.1039/c9mh00020h
10. Chen Q, Hu Q, Dukhovlinova E, et al. Photothermal therapy promotes tumor infiltration and antitumor activity of CAR T cells. *Adv Mater*. 2019;31:1900192. doi:10.1002/adma.201900192
11. Li W, Yang J, Luo L, et al. Targeting photodynamic and photothermal therapy to the endoplasmic reticulum enhances immunogenic cancer cell death. *Nat Commun*. 2019;10:3349. doi:10.1038/s41467-019-11269-8
12. Li X, Liu L, Wan Y, et al. Biodegradable π-conjugated oligomer nanoparticles with high photothermal conversion efficiency for cancer theranostics. *ACS Nano*. 2019;11:12901–12911. doi:10.1021/acsnano.9b05383
13. Chen WR, Adams RL, Higgins AK, Bartels KE, Nordquist RE. Photothermal effects on murine mammary tumors using indocyanine green and an 808-nm diode laser: an in vivo efficacy study. *Cancer Lett*. 1996;98:169–173. doi:10.1016/S0304-3835(06)80028-5
14. Ni G, Yang G, He Y, et al. Uniformly sized hollow microspheres loaded with polydopamine nanoparticles and doxorubicin for local chemo-photothermal combination therapy. *Chem Eng J*. 2020;379:122317. doi:10.1016/j.cej.2019.122317
15. Wan G, Cheng Y, Song J, et al. Nucleus-targeting near-infrared nanoparticles based on TAT peptide-conjugated IR780 for photochemotherapy of breast cancer. *Chem Eng J*. 2020;380:122458. doi:10.1016/j.cej.2019.122458
16. Zhang T, Jiang Z, Xve T, et al. One-pot synthesis of hollow PDA@DOX nanoparticles for ultrasound imaging and chemo-thermal therapy in breast cancer. *Nanoscale*. 2019;11(45):21759–21766. doi:10.1039/C9NR05671H
17. Dibaba ST, Caputo R, Xi W, et al. NIR light degradable antimony nanoparticle based drug delivery nanosystem for synergistic chemo-photothermal therapy in vitro. *ACS Appl Mater Interfaces*. 2019;11:48290–48299. doi:10.1021/acsami.9b20249
18. Zhang D, Zhang J, Li Q, et al. pH- and enzyme-sensitive IR820-paclitaxel conjugate self-assembled nanovehicles for near-infrared fluorescence imaging-guided chemo-photothermal therapy. *ACS Appl Mater Interfaces*. 2018;10:30092–30102. doi:10.1021/acsami.8b09098
19. Zaharie-Butucel D, Potara M, Suarasan S, Licarete E, Astilean S. Efficient combined near-infrared-triggered therapy: phototherapy over chemotherapy in chitosan-reduced graphene oxide-IR820 dye-doxorubicin nanoplatforms. *J Colloid Interface Sci*. 2019;552:218–229. doi:10.1016/j.jcis.2019.05.050
20. Xia B, Zhang Q, Shi J, Li J, Chen Z, Wang B. Co-loading of photothermal agents and anticancer drugs into porous silicon nanoparticles with enhanced chemo-photothermal therapeutic efficacy to kill multidrug-resistant cancer cells. *Colloids Surf B Biointerfaces*. 2018;164:291–298. doi:10.1016/j.colsurfb.2018.01.059
21. Li W, Peng JR, Tan LW, et al. Mild photothermal therapy/photodynamic therapy/chemotherapy of breast cancer by Lyp-1 modified docetaxel/IR820 co-loaded micelles. *Biomaterials*. 2016;106:119–133. doi:10.1016/j.biomaterials.2016.08.016
22. Pei P, Sun C, Tao W, Li J, Yang X, Wang J. ROS-sensitive thioketal-linked polyphosphoester-doxorubicin conjugate for precise phototriggered locoregional chemotherapy. *Biomaterials*. 2019;188:74–82. doi:10.1016/j.biomaterials.2018.10.010
23. Li Y, Lin J, Wang P, et al. Tumor microenvironment responsive shape-reversal self-targeting virus-inspired nanodrug for imaging-guided near-infrared-II photothermal chemotherapy. *ACS Nano*. 2019;11:12912–12928. doi:10.1021/acsnano.9b05425
24. Liu B, Wang W, Fan J, et al. RBC membrane camouflaged prussian blue nanoparticles for gamabutolin loading and combined chemo/photothermal therapy of breast cancer. *Biomaterials*. 2019;217:119301. doi:10.1016/j.biomaterials.2019.119301
25. Yang G, Zhou D, Pan Z, et al. Multifunctional low-temperature photothermal nanodrug with in vivo clearance, ROS-scavenging and anti-inflammatory abilities. *Biomaterials*. 2019;216:119280. doi:10.1016/j.biomaterials.2019.119280
26. Shim MK, Park J, Yoon HY, et al. Carrier-free nanoparticles of cathepsin B-cleavable peptide-conjugated doxorubicin prodrug for cancer targeting therapy. *J Controlled Release*. 2019;294:376–389. doi:10.1016/j.jconrel.2018.11.032
27. Ren C, Gao Y, Guan Y, et al. Carrier-free supramolecular hydrogel composed of dual drugs for conquering drug resistance. *ACS Appl Mater Interfaces*. 2019;11:33706–33715. doi:10.1021/acsami.9b12530
28. Feng B, Niu Z, Hou B, Zhou L, Li Y, Yu H. Enhancing triple negative breast cancer immunotherapy by ICG-templated self-assembly of paclitaxel nanoparticles. *Adv Funct Mater*. 2019;1906605. doi:10.1002/adfm.201906605
29. Zhou Z, Piao Y, Hao L, Wang G, Zhou Z, Shen Y. Acidity-responsive shell-sheddable camptothecin-based nanofibers for carrier-free cancer drug delivery. *Nanoscale*. 2019;11:15907–15916. doi:10.1039/c9nr03872h
30. Yang M, Zhao R, Fang Y, Jiang J, Yuan X, Shao J. Carrier-free nanodrug: a novel strategy of cancer diagnosis and synergistic therapy. *Int J Pharm*. 2019;570:118663. doi:10.1016/j.ijpharm.2019.118663
31. Lin J, Li C, Guo Y, et al. Carrier-free nanodrugs for in vivo NIR bioimaging and chemo-photothermal synergistic therapy. *J Mater Chem B*. 2019;7:6914–6923. doi:10.1039/c9tb00687g
32. Fan L, Zhang B, Xu A, et al. Carrier-free, pure nanodrug formed by the self-assembly of an anticancer drug for cancer immune therapy. *Mol Pharm*. 2018;15:2466–2478. doi:10.1021/acs.molpharmaceut.8b00444
33. Huang C, Hu X, Hou Z, Ji J, Li Z, Luan Y. Tailored graphene oxide-doxorubicin nanovehicles via near-infrared dye-lactobionic acid conjugates for chemo-photothermal therapy. *J Colloid Interface Sci*. 2019;545:172–183. doi:10.1016/j.jcis.2019.03.019
34. Maeda H. Toward a full understanding of the EPR effect in primary and metastatic tumors as well as issues related to its heterogeneity. *Adv Drug Deliv Rev*. 2015;91:3–6. doi:10.1016/j.addr.2015.01.002
35. Tsoi KM, MacParland SA, Ma XZ, et al. Mechanism of hard-nanomaterial clearance by the liver. *Nat Mater*. 2016;15:1212–1221. doi:10.1038/NMAT4718
36. Wang B, He X, Zhang ZY, Zhao Y, Feng WY. Metabolism of nanomaterials in vivo: blood circulation and organ clearance. *Acc Chem Res*. 2013;46:761–769. doi:10.1021/ar2003336
37. Su C, Liu Y, Li R, Wu W, Fawcett JP, Gu J. Absorption, distribution, metabolism and excretion of the biomaterials used in nanocarrier drug delivery systems. *Adv Drug Deliv Rev*. 2019;143:97–114. doi:10.1016/j.addr.2019.06.008